Accepted Article

# Origin of ...ation at the ...ina:

X... ...Tao Ye

**Abstrac...** ...ssociated with the ...portant role in our underst... ...this contribution, the Neopr... ...China was identified. Magn... ...l with chert. The BIF conta... ...rth elements (LREEs) base... ...tion, the BIF exhibits slig... ...nalies, chondritic Y/Ho rati... ...o 1.46, averaging 0.37). Al... ...closely related to the su... ...r, the Baijianshan BIF is ...$Fe_{IRMM-014}$ values ranging ...e precipitation of this BIF. ...ciated with a significantly ...e by a local ice sheet. This ...or even lower than that of

...tope, Tarim block

...ources in the world, are typical ... BIF was firstly defined as a type ...1966), which was later revised as ...equivalent) alternating with layers ...anging from 20% to 35% (James, ... and then a large number of BIFs ...peak at ca. 2.5 Ga (Klein, 2005 and ...urred in the Neoproterozoic (0.8-0.6 ...epted that the precipitations of BIFs .../or oceanic oxygen levels (i.e., Great ...he source of the hydrothermal fluids, ...Holland, 2002). In line with tectonic ...nd Superior-type (Gross, 1980), the ..., in the sequences mainly composed of ... 1992; Li et al., 2014; Sial et al., 2015), ...ry rock in shallow marine environment,

...n much less than those of Archean and ...ch as Rapitan BIF in Canada (Halverson et ...et al., 2011), Sawawin BIF in Saudi Arabia ...011), Holowilena and Oraparinna in South ... in California (Lechte et al., 2018) and Wadi ...l., 2020). They were also discovered in the ... South China, such as Sanjiang in Guangxi ... et al., 2014), Xinyu in Jiangxi Province (Li et ...ong in the Central Tianshan (Lei et al., 2016, ...orogenic belt (Hu et al., 2017, 2020). Several

These samples are dominated by magnetite an
mesoband (mm- to cm-scale) and microban
magnetite, quartz, rare hematite, siderite,
minerals, such as chlorite (Fig. 3g) and se
the bedding.

The shallow gray tuffs under th
Nevertheless, the sub-euhedral or
mm, can be seen under magnif
sample was collected from
(

The blackish green b
The minerals in the
oxide can be obs
geochemical an

**4 Analytic**

**4.1**

**4.2**

Sever
location. Wi
fused glass beads
Survey), following the p
uncertainties are between 1 and
$Fe_2O_3$, with the procedures described
supplementary Table 2.

Trace elements were determined using a Perkin-Elmer Sc
atory of Ore Deposit Geochemistry, Institute of Geochemis
alytical accuracy better than 5%. Samples were d
PTFE-lined stainless steel bombs at 190
better than 1% with co
pplementary Table 2.

lass Isoprobe Mi
Institut
similar to th
for mass-fractio
values for the NBS
$^{143}Nd/^{144}Nd$ = 0.512115. All
depositional age (737 Ma) for th

Iron isotope ratios were m
Ltd. The results of Fe iso
the standard sample is

ina Geological Su
Measured $^{87}Sr/^{86}Sr$ an
.1194 and $^{146}Nd/^{144}Nd$ = 0.
dard $^{87}Sr/^{86}Sr$ = 0.71025 and
itial $^{143}Nd/^{144}Nd$ values of the BIF a
iijianshan BIF.

MC-ICP-MS at Beijing Createch Tes
he ten thousandth deviation of t

with 1ml
2h (Qi et al., 2000). The a
ns > 200 ppm, and 1-3% when less

Accepted

Accepted Artic

## 5 Analytical Results

### 5.1 Zircon U-Pb age

Zircons from the tuff sample 2071 are variable in size with the length varying from 60 μm to 150 μm and the aspect ratios 1-2. In CL images most zircon exhibit oscillatory zoning, sharing the features of the zircons crystallized from silicic magma (Wu and Zheng, 2004). Thirty-two analyses were conducted on 32 zircon grains and the results are presented in supplementary Table 1 and illustrated in Fig. 4. Obviously, some analyses show variable radiogenetic lead lost. However, the results can be broadly divided into two sub-groups. Group 1, which is likely to be xenocrystal and generally have larger size, constructs a good Discordia with upper intercepted age of 1378±44 Ma (MSWD=5.8). Group 2 mostly shows euhedral in form and smaller in size. Twenty-one analyses construct a good Discordia with an intercepted age of 736.2±3.8 Ma (N=21, MSWD=1.08) (insert of Fig. 4). Excluded the significant discordant analyses, the left fifteen analyses of well concordance between $^{206}Pb/^{238}U$ age and $^{207}Pb/^{235}U$ age, yield a mean $^{206}Pb/^{238}U$ age of 737.0±4.0 Ma (N=15, MSWD=0.20). This age is interpreted as the deposition time of the Baijianshan BIF.

### 5.2 Whole rock Geochemistry

#### 5.2.1 Geochemistry of the basalts

Three basalt samples (2702H1, 270H2 and 2702H3) have low $SiO_2$ contents (39.93% to 44.55%). The incompatible elements for the rock type classification are used due to the high LOI. Their high Nb/Y ratios (1.05-1.09) define their alkaline signature and in the Nb/Y vs. $Zr/TiO_2$ diagram, they plot into the alkaline basalt field (Figure not shown). With respect to the trace elements, they have REE ranging from 186 ppm to 195 ppm and show variable LREE enriched Chrondrite-normalized pattern (Fig. 5a) ($La_N/Yb_N$ = 9.8-11.0). In line with their low Cr (214-306 ppm) and Ni contents (162-216.9 ppm), the basalts are evolved magma. However, the primitive mantle-normalized diagram shares most features of the OIB-like basalts with insignificant Nb-Ta trough (Nb/La = 1.0-1.1) (Figure not shown).

#### 5.2.2 Geochemistry of the BIF

As shown in supplementary Table 2, the samples from Baijianshan BIF are rich in $Fe_2O_3^T$ and $SiO_2$. $Fe_2O_3^T$ concentrations vary between 13.11% and 56.65% (38.44% on average), whereas $SiO_2$ varies between 26.81% and 55.06% (42.02% on average). They have low contents of $Al_2O_3$ (1.56%-7.58%, 3.66% on average), $TiO_2$, MnO, $P_2O_5$, CaO, $Na_2O$, $K_2O$ and variable total rare earth elements and other incompatible elements (supplementary Table 2).

Their REE abundances vary from 38.1 ppm to 150.8 ppm. Normalized against Post Archean Average Shale (PAAS; McLennan, 1989), they are characterized by depletion of LREE relative to HREE with the $La_N/Yb_N$ of 0.23-0.69 (Fig. 5b). The REY patterns exhibit no Ce and Pr anomalies (the combination of $Ce/Ce^* \sim 1$ and $Pr/Pr^* \sim 1$; Bau and Dulski, 1996) and insignificant Eu and Y anomaly ($Eu/Eu^*$ = 0.96-1.14; Y/Ho ratios ranging from 23.3 to 31.8 with an averaged value of 26.39, Table 2).

#### 5.2.3 Sr-Nd isotope compositions

Sr-Nd concentrations and isotopic ratios of the Baijianshan BIF and basalts are presented in supplementary Table 3. As for the basalts, the basalts exhibit high initial Sr isotope compositions with $(^{87}Sr/^{86}Sr)_i$ ranging from 0.7061 to 0.7084 due to post-eruption hydrothermal alteration. In addition,

6.9.

Strontium and neodymium concentrations of Baijianshan BIF range from 20.3 ppm to 256 ppm and from 7.06 ppm to 59.8 ppm, respectively. The nine samples have a large range of measured $^{143}Nd/^{144}Nd$ (0.51231-0.51243) and $^{87}Sr/^{86}Sr$ (0.7179- (t = 737Ma) values range from -0.45 to 1.46, with an average of 0.37. However, the BIF samples exhibit a large range of the $(^{87}Sr/^{86}Sr)_i$ values between 0.6412 and 0.7175, possibly due to the post-deposition hydrothermal alteration and the large range of Rb/Sr ratios varying from 0.02 to 3.47.

#### 5.2.4 Fe isotope compositions

The Fe isotope compositions of the Baijianshan BIF samples are presented in supplementary Table 4. The six samples yield $^{56}Fe_{IRMM-014}$ values of 1.24- $^{57}Fe_{IRMM-014}$ values of 1.78- Their enrichment in heavy Fe isotopes shares the signatures of the Neoproterozoic BIFs (Halverson et al., 2011; Yan et al., 2011; Shen et al., 2018).

## 6 Discussions

### 6.1 Iron sources for the Baijianshan BIFs

Field and microscopic observations revealed that the Neoproterozoic Baijianshan BIF has not

experienced significant metamorphism (Fig. 3b, c and d), indicating the original geochemical characteristics were well retained and can be used to decipher the iron sources and the oceanic environments when it precipitated.

The Baijianshan BIF shows a modern seawater REE signature with significant LREE depletion relative to the HREE ($La_N/Yb_N$ = 0.41) (Fig. 5b, Zhang and Nozaki, 1996; Alibo and Nozaki, 1999). A range of factors can affect the primary REY composition in terms of BIF depositional processes, including post-depositional metamorphism and/or syn-deposition clastic contamination (Alexander et al., 2008; Hu et al., 2020). Previous studies demonstrated that diagenetic and metamorphic events (such as weathering and/or fluid-rock interactions) have negligible effects on the REY of the chemical sediments (Bolhar et al., 2004). However, Rb is a relatively mobile element compared to highly immobile elements such as Th. In Fig. 6a, the well positive correlation between Rb and Th demonstrates insignificant mobility of the LILEs (Large Ion Lithophile Elements) and the absence of significant diagenetic or metamorphic alteration effects, this conclusion is also consistent with thin section observations (Fig. 3c, d, g, h). With respect to the syn-depositional processes, the contents of $Al_2O_3$ and $TiO_2$ are consistently low with averages of 3.66% and 0.41%. In addition, despite the positive correlations between $Al_2O_3$ and $TiO_2$ (r = 0.93), $K_2O$ (r = 0.79), Rb (r = 0.78), V (r = 0.45), Sc REE (r = 0.62) (Fig. 6b-i) signify the incorporation of terrigenous contribution in the deposition processes, most correlation coefficients are much lower than those BIFs sourced from recycled crust (Basta et al., 2011; Cox et al., 2013; Hu et al., 2017, 2020). Besides, the Baijianshan BIF shares similar REE patterns with those BIFs from North China Craton but contains slightly higher contents of $Al_2O_3$ and $TiO_2$ (Li et al., 2014). Taken together, we suggest a little incorporation of terrigenous component in the Baijianshan BIF.

Positive Eu anomalies are generally interpreted as the precipitation of high-temperature hydrothermal fluids (Danielson et al., 1992; Bau and Dulski, 1999) while low-temperature hydrothermal fluids usually display weak or no Eu anomalies (Michard et al., 1993; Li et al., 2014). Most samples from the Baijianshan BIF show negligible Eu anomalies ($Eu/Eu^*$ = 0.96~1.14, averaging 1.07), which are indicative of low-temperature hydrothermal solutions (Danielson et al., 1992). The (t) value can be used as a tracer to distinguish different sources and crustal contamination. As shown in Fig. 7, the Baijianshan BIF has slightly average (t) value (average of 0.37), much lower than those of Baijianshan basalt, indicating that the deposition of the Baijianshan BIF was controlled by a hydrothermal flux with mantle- (Jacobsen and Pimentel-Klose, 1988). However, the slightly negative correlation between Ma) and $Al_2O_3$ contents (Fig. 8a) argues for the low proportion of detrital components inputting.

The Y/Ho ratios of BIFs can provide constraints of the material source and precipitation environment of BIFs (Hu et al., 2017). Modern seawaters have a Y/Ho ratio of 44-74 (Bau and Dulski, 1996). The terrestrial material has a Y/Ho ratio of ~26, any little terrestrial contamination could quickly descend seawater-like superchondretic Y/Ho ratios (>44) (Bolhar et al., 2004). The hydrothermal fluids have almost chondritic Y/Ho ratios (26-28, Douville et al., 1999; Bau and Dulski, 1999). The Baijianshan BIF has a range of Y/Ho ratios between 23 and 32, similar to the chondritic values (26-28, Bau and Dulski, 1999), possibly due to the mixture of high and/or low-T hydrothermal fluids (Hu et al., 2020). Y/Ho ratios of the Baijianshan BIF samples might inherit from the low-T hydrothermal fluids, but the influences of terrestrial materials can not be completely excluded. Compared with the BIFs in North China Craton, the Baijianshan BIF displays relatively low positive Eu anomalies, low Y/Ho ratios as well as a slighly depleted Li et al., 2014; Wang et al., 2016), illustrating the input of low-temperature hydrothermal fluids during the deposition of the Baijianshan BIF.

T013

Accepted

Bald
frac
Acta
Basta, F.F.,
formation
Neoproterozoi
Bau, M., Dulski, P.
iron-formations, Trans
Bau, M., Dulski, P., 1999. Co
implications for Y and REE be
Chem. Geol. 155, 77-90.
Bolhar, R., Kamber, BS., Moorbath, S., Fed
chemical sediments by trace element signatures.
Bullen, T.D., White, A.F., Childs, C.W., Vivit, D.V., Schu
isotope fractionation. Geology 29, 699-702.
Byrne, R., Sholkovitz., 1996. Marine chemistry and geochemistry of th
Eyring, L. (Eds.), Handbook on the Physics and Chemistry of the Rare Earths. Else
Cailteux, J.L.H., Kampunzu, A.B.H., Batumike, M.J., 2005. Lithostratigraphic position
-
Journal of African Earth Sciences 42, 82-94.
Canfield, D.E., Poulton, S.W., Knoll, A.H., Narbonne, G.M., Ross, G., Goldberg, T., Strauss, H., 2008. Ferruginous Conditions Dominated Later Neoproterozoic Deep-Water Chemistry. Science 321(5891), 949-952.
Chen, D.Z., Wang, J.G., Qing, H.R., Yan, D.T., Li, R.W., 2009. Hydrothermal venting activities in the Early

Accepted Article

Cambrian, South China: Petrological, geochronological and stable isotopic constraints. Chemical Geology 258, 168-181.
Cox, G.M., Halverson, G.P., Minarik, W.G., Heron, D.P.L., Macdonald, F.A., Bellefroid, E.J., Strauss, J.V., 2013. Neoproterozoic iron formation: an evaluation of its temporal, environment al and tectonic significance. Chem. Geol. 362, 232-249.
Cox, G.M., Halverson, G.P., Poirier, A., Le Heron, D., Strauss, J.V., Stevenson, R., 2016. A model for Cryogenian iron formation. Earth Planet. Sci. Lett. 433, 280-292.
Danielson, A., Moller, P., Dulski, P., 1992. The europium anomalies in banded iron formations and the thermal history of the oceanic crust. Chem. Geol. 97, 89-100.
Dauphas, N., van Zuilen, M., Wadhwa, M., Davis, A.M., Marty, B., Janney, P.E., 2004. Clues from Fe isotope variations on the origin of early Archean BIFs from Greenland. Science 306, 2077-2080.
EI-Rahman, Y.A., Gutzmer, J., Li, X.H., Seifert, T., Li, C.F., Ling, X.X., Li, J., 2020. Not all Neoproterozoic iron formations are glaciogenic: Sturtian-aged non-Rapitan exhalative iron formations from the Arabian-Nubian Shield. Mineralium Deposita 55, 577-596.
Feng, L.J., Huang, J., Lu, D.B., Zhang, Q.R., 2016. Major and trace element geochemistry of the Neoproterozoic syn-glacial Fulu iron formation, South China. Geological Magazine 154, 1-10.
Freitas, B.T., Warren, L.V., Boggiani, P.C., Almeida, R.P.D., Piacentini, T., 2011. Tectono-sedimentary evolution of the Neoproterozoic BIF-bearing Jacadigo Group, SW-Brazil. Sedimentary Geology 238, 48-70.
Grassineau, N.V., Nisbet, E.G., Bickle, M.J., Fowler, C.M.R., Lowry, D., Mattey, D.P., Abell, P., Martin, A., 2000. Antiquity of the biological sulphur cycle: evidence from sulphur and carbon isotopes in 2700 million-year-old rocks of the Belingwe Belt, Zimbabwe. Proc. R. Soc. Lond. B 268, 113-119.
Gross, G.A., 1980. A classification of iron-formation based on depositional environments. Canadian Mineralogist 18, 215-222.
Gross, G.A., Mcleod, C.R., 1980. A preliminary assessment of the chemical composition of iron formation in Canada. Canadian Mineralogist 18, 223-229.
Halverson, G.P., Poitrasson, F., Hoffman, P.F., Nédélec, A., Montel, J.M., Kirby, J., 2011. Fe isotope and trace element geochemistry of the Neoproterozoic syn-glacial Rapitan iron formation. Earth Planet. Sci. Lett. 309(1), 100-112.
Hoffman, P.F., Kaufman, A.J., Halverson, G.P., Schrag, D.P., 1998. A Neoproterozoic snowball Earth. Science 281, 1342-1346.
Hoffman, P.F., Schrag, D.P., 2002. The snowball earth hypothesis: testing the limits of global change. Terra Nova 14(3), 129-155.
Hoffmann, K.H., Condon, D.J., Bowring, S.A., Prave, A.R., Fallick, A., 2006. Lithostratigraphic, carbon ( $^{13}C$) isotope and U-Pb zircon age constraints on early Neoproterozoic (ca. 755 Ma) glaciation in the Gariep Belt, southern Namibia. Snowball Earth Conference, July 16-21, 2006, Montle Namibia, Ticino, Switzerland, 51.
Holland, H.D., 2002. Volcanic gases, black smokers, and the great oxidation event. Geochimica et Cosmochimica Acta 66(21), 3811-3826.
Hou, K.J., Li, Y.H., Gao, J.F., Liu, F., Qin, Y., 2014. Geochemistry and Si-O-Fe isotope constraint on the origin of banded iron formations of the Yuanjiacun Formation, Lvliang Group, Shanxi, China. Ore Geology Reviews 57, 288-298.
Hu, J., Wang, H., Wang, M., 2017. Geochemistry and origin of the Neoproterozoic Dahongliutan banded iron formation (BIF) in the Western Kunlun orogenic belt, Xinjiang (NW China). Ore Geology Reviews 89, 836-857.
Hu, J., Wang, H., Zhang, L.G., 2020. A rare earth element and Nd isotopic investigation into the provenance and deposition of the Dahongliutan banded iron formation and associated carbonates, NW China: Implications on Neoproterozoic seawater compositions. Precambrian Research 342, 1-29.
Jackson, S.E., Pearson, N.J., Griffin, W.L., Belousova, E.A., 2004. The application of laser ablation-inductively coupled plasma-mass spectrometry to in situ U  Pb zircon geochronology. Chemical Geology 211(1-2), 47-69.
Jacobsen, S.B., Pimentel-Klose, M.R., 1988. Nd isotopic variations in Precambrian banded iron formations. Geophys Res Lett 15, 393-396.
James, H.L., 1954. Sedimentary facies of iron-formation. Economic Geology 49(3), 235-293.
James, H.L., 1966. Chemistry of the iron-rich sedimentary rocks. U.S. Geol. Survey Prof, 440-461.
James, H.L., 1983. Distribution of banded iron-formation in space and time. Developments in Precambrian Geology 6, 471-490.
Johnson, C.M., Beard, B.L., Beukes, N.J.,
Earth as inferred from Fe isotope studies of banded iron formations from the Transvaal Craton. Contributions to Mineralogy and Petrology 144(5), 523-547.
Johnson, C.M., Beard, B.L., Klein, C., Beukes, N.J., Roden, E.E., 2008. Iron isotopes constrain biologic and abiologic processes in banded iron formation genesis. Geochimica Et Cosmochimica Acta 72(1), 151-169.
Johnson, C.M., Skulan, J.L., Beard, B.L., Sun, H., Nealson, K.H., Braterman, P.S., 2002. Isotopic fractionation between Fe(Ⅲ) and Fe(Ⅱ) in aqueous solution. Earth Planet Sci Lett 195, 141-153.
Johnston, D.T., Poulton, S.W., Dehler, C., Porter, S., Husson, J., Canfield, D.E., Knoll, A.H., 2010. An emerging picture of Neoproterozoic ocean chemistry: insights from the Chuar Group, Grand Canyon, USA. Earth Planet. Sci. Lett. 290, 64-73.
Kay, R.M., Liyungu, A.K., Njamu, F.M., Somwe, V., Banda, J., Mosley, P.N., Armstrong, R.A., 2001. The western arm of the Lufilian Arc in NW Zambia and its potential for copper mineralization. Journal of African Earth Sciences 33, 503-528.
Klein, C., 2005. Some Precambrian banded iron-formations (BIFs) from around the world: Their age, geologic setting, mineralogy, metamorphism, geochemistry, and origins. American Mineralogist 90(10), 1473-1499.
Klein, C., Beukes, N.J., 1992. Time distribution, stratigraphy, sedimentologic setting, and geochemistry of Precambrian iron-formations. In: Schopf, J.W., Klein, C. (Eds.), The Proterozoic Biosphere. Cambridge University Press, Cambridge, 139-146.
Klein, C., Ladeira, E.A., 2004. Geochemistry and mineralogy of Neoproterozoic banded iron-formations and some selected, siliceous manganese formations from the Urucum district, Mato Grosso do Sul, Brazil. Econ. Geol. 99, 1233-1244.
Konhauser, K.O., Kappler, A.K., Roden, E.E., 2011. The microbial role in iron redox and biomineralization reactions. Elements 7, 89-93.

change. Precambr. Res. 239, 79-94.
Sun, S.S., McDonough, W.F., 1989. Chemical and isotopic systematics of oceanic basalts: Implications for mantle composition and processes. Geological Society London Special Publications 42(1), 313-345.
Tang, S.H., Zhu, X.K., Li, J., Yan, B., Li, S.Z., Li, Z.H., Wang, Y., Sun, J., 2016. New Standard Solutions for Measurement of Iron, Copper and Zine Isotope Compositions by Multi-collector Inductively Coupled Plasma-Mass Spectrometry. ROCK AND MINERAL ANALYSIS 35(2), 127-133 (in Chinese with English abstract).
Wu, Y.B., Zheng, Y.F., 2004. A study on the genetic mineralogy of zircon and its restriction on the interpretation of U-Pb age. CHINESE SCIENCE BULLETIN 49(16), 1589 (in Chinese).
Xinjiang Bureau of Geology and Mineral Resources (BGMR), 1993. Regional Geology of Xinjiang Uygur Autonomous Region. Geological Publishing House, Beijing, 8-33 (in Chinese).
Xu, B., Xiao, S.H., Zou, H.B., Chen, Y., Li, Z.X., Song, B., Liu, D.Y., Zhou, C.M., Yuan, X.L., 2009. SHRIMP zircon U-Pb age constraints on Neoproterozoic Quruqtagh diamictites in NW China. Precambrian Research 168, 247-258.
Xu, B., Zou, H.B., Chen, Y., He, J.Y., Wang, Y., 2013. The Sugetbrak basalts from northwestern Tarim Block of northwest China: Geochronology, geochemistry and implications for Rodinia breakup and ice age in the Late Neoproterozoic. Precambrian Research 236, 214-226.
Xu, D.R., Wang, Z.L., Chen, H.Y., Hollings, Pete, Jansen, Nicholas, H., Zhang, Z.C., Wu, C.J., 2014. Petrography and geochemistry of the Shilu Fe Co Cu ore district, South China: Implications for the origin of a Neoproterozoic BIF system. Ore Geology Reviews 57, 322-350.
Xu, Z.Q., He, B.Z., Zhang, C.L., Zhang, J.X., 2013. Tectonic framework and crustal evolution of the Precambrian basement of the Tarim Block in NW China: New geochronological evidence from deep drilling samples. Precambrian Research 235, 150-162.
Yan, B., Zhu, X.K., Tang, S.H., Zhu, M.Y., 2010. Fe isotopic characteristics of the Neoproterozoic BIF in Guangxi Province and its Implications

Accepted Article

**Figure captions**

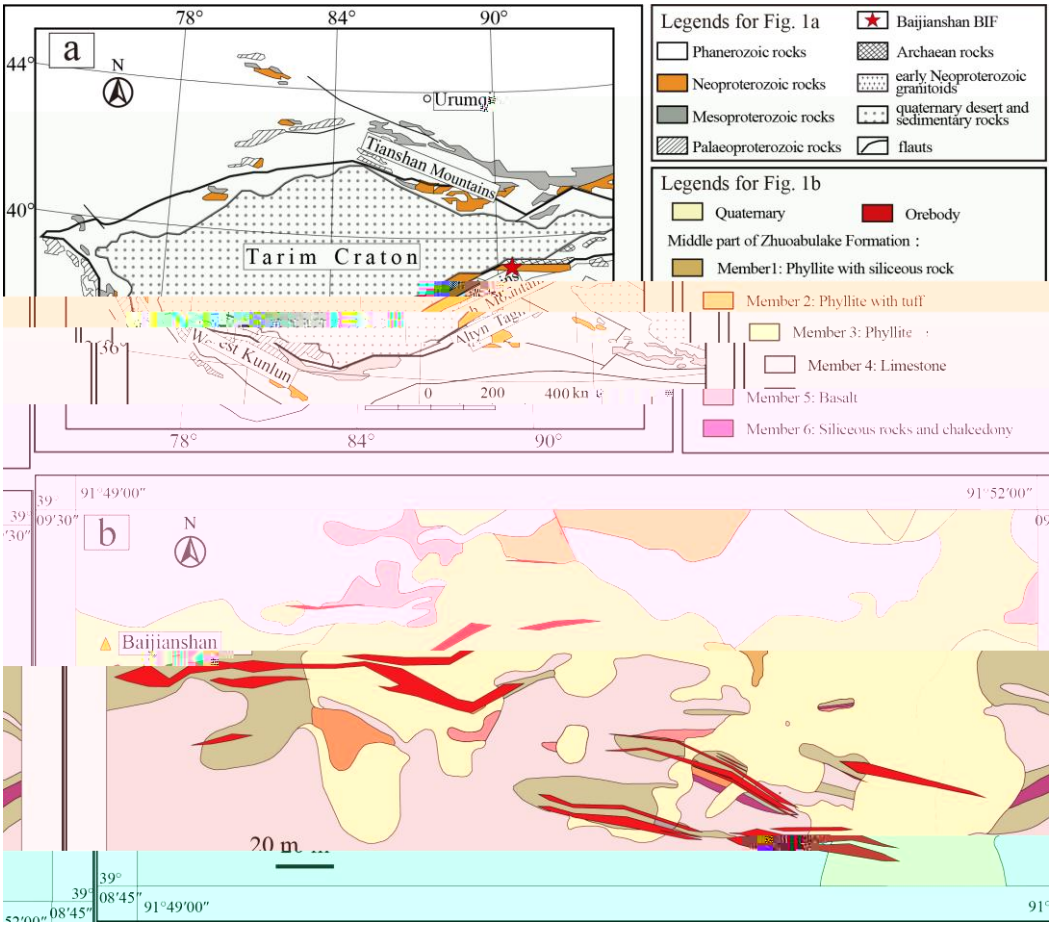


Fig. 1 (a) Sketch Precambrian geological map of Tarim Craton, showing the location of the Baijianshan BIF (modified after Lu et al., 2008). (b) Geological map of the Baijianshan Banded Iron Formation (Baijianshan BIF).

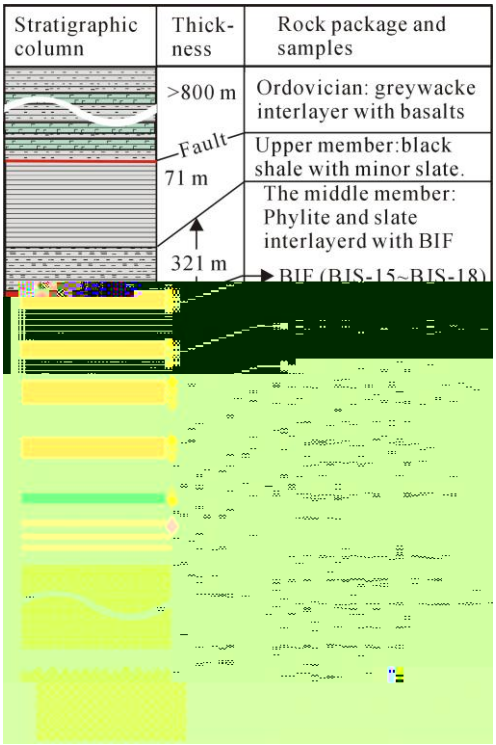


Fig. 2 Stratigraphical column of the Baijianshan BIF.

Accepted Article

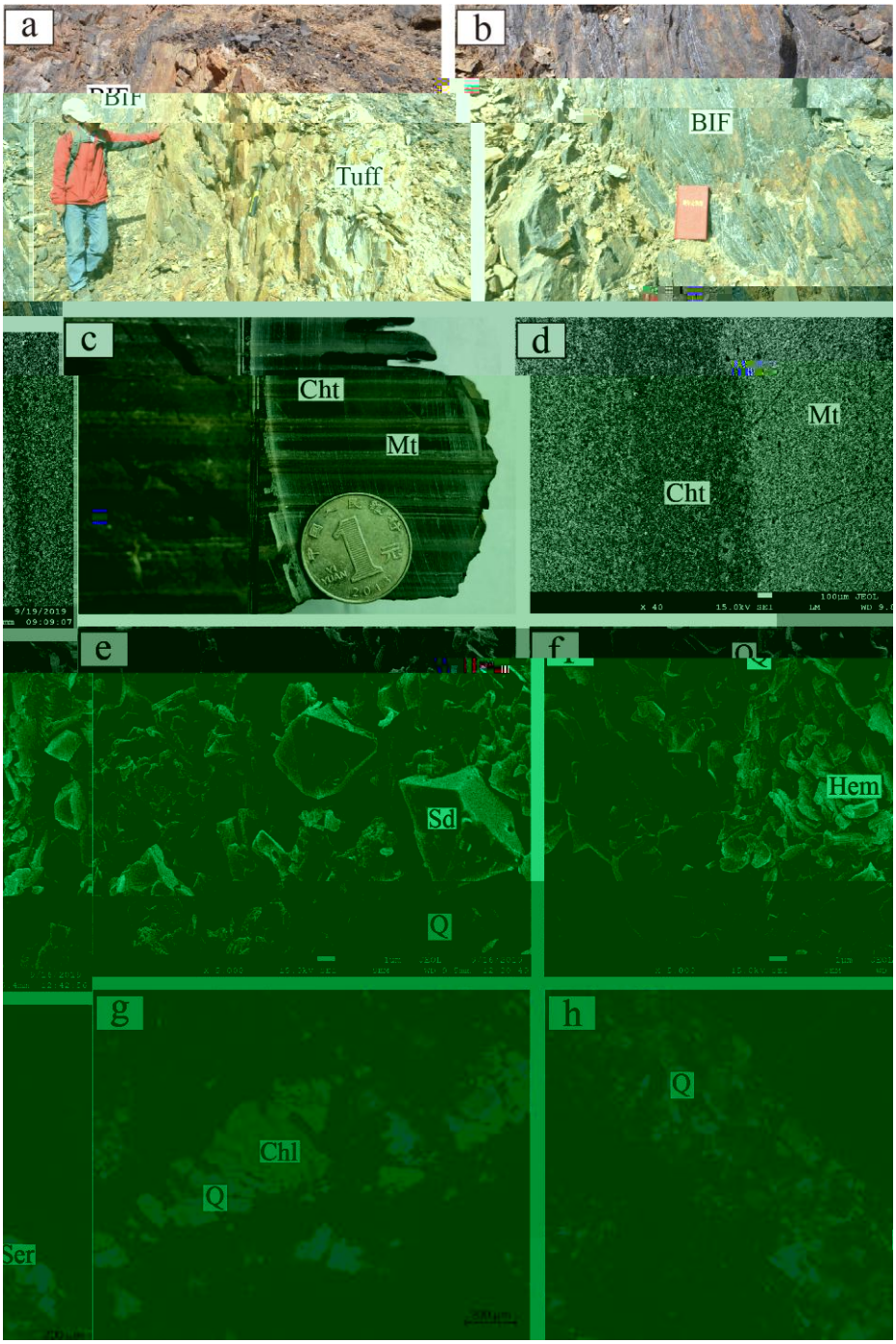


Fig. 3 Field photographs, hand specimen and mineral features of the Baijianshan BIF. (a) The tuff layers in the Baijianshan BIF. (b) Laminated Fe orebodies with local bend. (c) hand specimen. (d) Scanning electron microscopy (SEM) images. Detailed petrographic examination by SEM and transmitted light showing mineral assemblage: (e) Siderite. (f) Hematite. (g) Chlorite. (h) Sericite. Cht = Chert, Mt = Magnetite, Sd = Siderite, Q = Quartz, Hem = Hematite, Chl = Chlorite, Ser = Sericite.

Accepted Artic

Fig. 4 Concordia diagram of the zircon U-Pb ages of the tuff at the Baijianshan BIF.

Fig. 5 (a) Chondrite-normalized REE parttern of the basalts. Chondrite-normalized values after Sun and McDonough (1989). (b) PAAS-normalized REE+Y diagrams of BIFs from the Baijianshan BIF. The grayish zone represents the REY data from the Xinyu BIF (Li et al., 2014). PAAS-normalized values after McLennan (1989).

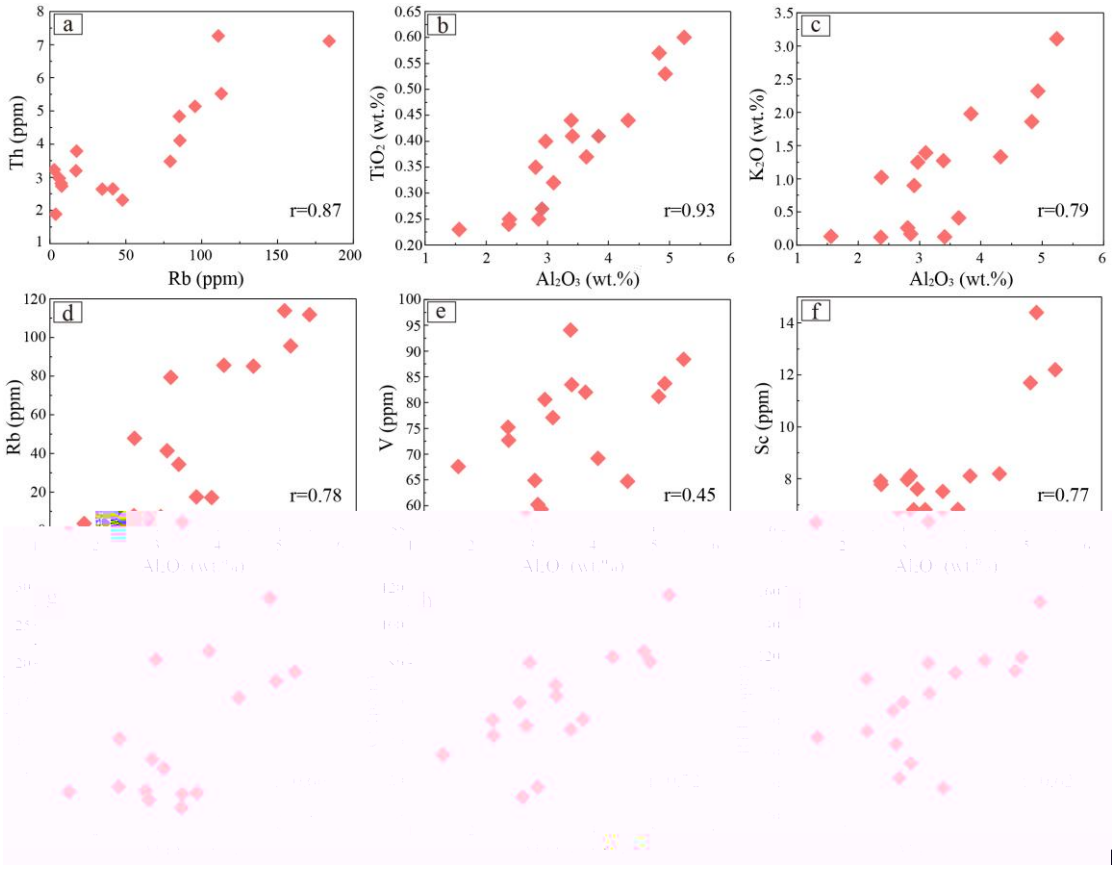


Fig. 6 (a) Bi-variation n between Rb and Th of Baijianshan BIF samples; (b-i) Bi-variation between $Al_2O_3$ and $TiO_2$ (b), $K_2O$ (c), Rb (d), V (e), Sc (f), Cs (g), Cr (h) and REE (i) of the Baijianshan BIF. Data for bulk-rock BIF samples are listed in supplementary Table 2.

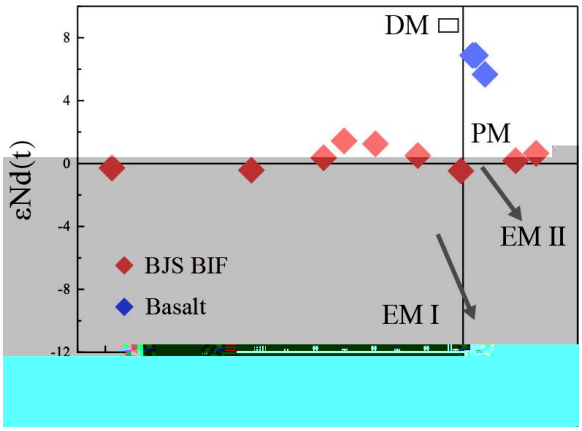


Fig. 7 $^{87}Sr/^{86}Sr)_i$ diagram of BIF and basalt samples in Baijianshan.

AC

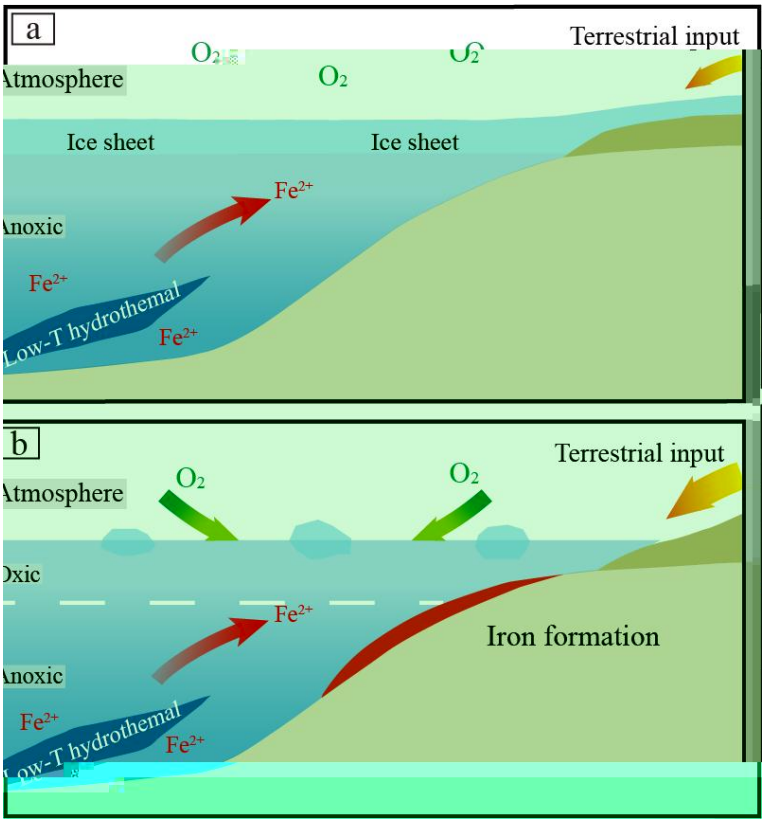


Fig. 12 Cartoon model of the formation of the Baijianshan BIF (see details in the text).

## Appendix Table Captions

Appendix-Table 1 LA-ICP-MS U-Pb data for zircon from tuff in the first section of the Lapeiquan Formation

Appendix-Table 2 Geochemical compositions of the Baijianshan BIF

Appendix-Table 3 Sr-Nd isotopic data of the Baijianshan BIF

Appendix-Table 4 Fe isotopic data of the Baijianshan BIF

**Supplementary Table 1 Zircon U-Pb age data of the tuff from the Baijianshan BIF**

| Spot | U ppm | Th ppm | Th/U | $^{206}Pb/^{238}U$Age | | $^{207}Pb/^{235}U$Age | | $^{207}Pb/^{206}Pb$ | | $^{207}Pb/^{235}U$ | | $^{206}Pb/^{238}U$ | |
|---|---|---|---|---|---|---|---|---|---|---|---|---|---|
| 2071-1 | 3079 | 831 | 0.27 | 1335 | 14 | 1360 | 21 | 0.0887 | 0.0012 | 2.8156 | 0.0427 | 0.2301 | 0.0025 |
| 2071-2 | 805 | 427 | 0.53 | 898 | 11 | 1154 | 20 | 0.1027 | 0.0014 | 2.1169 | 0.0369 | 0.1495 | 0.0018 |
| 2071-3 | 529 | 381 | 0.72 | 776 | 8 | 1009 | 18 | 0.0965 | 0.0016 | 1.7019 | 0.0307 | 0.1279 | 0.0014 |
| 2071-4 | 155 | 81 | 0.52 | 835 | 9 | 1350 | 22 | 0.1458 | 0.0022 | 2.778 | 0.0462 | 0.1382 | 0.0015 |
| 2071-5 | 184 | 101 | 0.55 | 751 | 8 | 1009 | 18 | 0.0999 | 0.0016 | 1.7022 | 0.0304 | 0.1236 | 0.0013 |
| 2071-6 | 297 | 252 | 0.85 | 1273 | 14 | | | | | | | | |

**Supplementary Table 2 Geochemical compositions of Baijianshan BIF**

| Sample | BJS-1 | BJS-2 | BJS-3 | BJS-4 | BJS-5 | BJS-6 | BJS-7 | BJS-8 | BJS-9 | BJS-10 |
|---|---|---|---|---|---|---|---|---|---|---|
| Major elements (%) | | | | | | | | | | |
| $Fe_2O_3$ | 53.60 | 41.52 | 56.64 | 52.26 | 30.01 | 36.85 | 41.01 | 45.22 | 39.78 | 48.55 |
| $SiO_2$ | 29.91 | 38.96 | 26.81 | 31.20 | 40.92 | 40.79 | 36.97 | 41.77 | 43.66 | 37.59 |
| $Al_2O_3$ | 1.56 | | | | | | | | | |

Accepted Article

| | | | | | | | | | | |
|---|---|---|---|---|---|---|---|---|---|---|
| $TFe_2O_3$ | 21.79 | 28.86 | 44.82 | 42.63 | 26.98 | 13.11 | 40.45 | 11.61 | 11.70 | 11.98 |
| $SiO_2$ | 55.06 | 49.87 | 41.24 | 43.65 | 53.64 | 59.90 | 42.80 | 39.94 | 40.91 | 44.55 |
| $Al_2O_3$ | 5.24 | 4.93 | 2.81 | 2.86 | 4.83 | 7.58 | 3.84 | 11.36 | 11.45 | 10.76 |
| CaO | 0.81 | 1.02 | 0.75 | 0.75 | 0.76 | 0.84 | 0.65 | 9.77 | 9.31 | 7.45 |
| MgO | 1.57 | 1.51 | 0.74 | 0.86 | 1.36 | 2.32 | 1.31 | 8.40 | 8.54 | 10.38 |
| $TiO_2$ | 0.60 | 0.53 | 0.35 | 0.25 | 0.59 | 0.86 | 0.41 | 3.66 | 3.80 | 3.60 |
| MnO | 0.03 | 0.04 | 0.05 | 0.03 | 0.03 | 0.02 | 0.03 | 0.24 | 0.25 | 0.23 |
| $P_2O_5$ | 0.20 | 0.35 | 0.49 | 0.40 | 0.23 | 0.19 | 0.54 | 0.46 | 0.43 | 0.38 |
| $K_2O$ | 3.11 | 2.32 | 0.26 | 0.17 | 1.86 | 3.78 | 1.98 | 1.35 | 1.27 | 0.36 |
| $Na_2O$ | 0.94 | 1.25 | 0.14 | 0.19 | 0.63 | 0.77 | 0.88 | 0.94 | 0.98 | 0.59 |
| LOI | 2.06 | 1.97 | 4.57 | 2.89 | 2.9 | 3.19 | 1.92 | 12.02 | 11.39 | 9.60 |
| FeO | 7.97 | 7.26 | 3.89 | 5.29 | 6.06 | 6.57 | 5.31 | - | - | - |
| Total | 99.38 | 99.91 | 100.11 | 99.97 | 99.87 | 99.13 | 100.12 | 99.75 | 100.03 | 99.88 |
| Trace elements (ppm) | | | | | | | | | | |
| Cr | 118 | 81.0 | 59.7 | 10.5 | 86.2 | 112 | 50.9 | 214 | 214 | 306 |
| Ni | 15.6 | 14.5 | 12.1 | 11.0 | 15.6 | 12.3 | 12.6 | 162 | 166 | 217 |
| Co | 76.1 | 70.2 | 33.7 | 34.7 | 54.0 | 27.1 | 45.3 | 48.0 | 62.9 | 50.7 |
| Sc | 12.2 | 14.4 | 7.97 | 8.11 | 11.7 | 15.1 | 8.11 | 26.4 | 26.1 | 25.7 |
| Ba | 662 | 562 | 111 | 19.2 | 359 | 1219 | 385 | 877 | 864 | 296 |
| Sr | 45.0 | 53.3 | 45.8 | 26.1 | 32.6 | 37.0 | 48.9 | 205 | 209 | 150 |
| Rb | 111 | 95.6 | 7.36 | 6.13 | 113 | 184 | 85.6 | 34.4 | 32.2 | 12.3 |
| Zr | 101 | 93.4 | 60.0 | 87.9 | 79.9 | 116 | 79.7 | 259 | 251 | 228 |
| Hf | 2.63 | 2.37 | 1.23 | 1.50 | 2.11 | 2.99 | 1.92 | 5.35 | 5.74 | 6.00 |
| Ta | 0.88 | 0.75 | 0.37 | 0.36 | 0.64 | 0.84 | 0.53 | 2.24 | 2.33 | 2.14 |
| Ga | 7.95 | 7.63 | 4.39 | 4.63 | 7.12 | 10.3 | 5.97 | 18.3 | 17.2 | 18.8 |
| Cu | 27.6 | 21.6 | 8.12 | 3.56 | 21.4 | 36.0 | 12.4 | - | - | - |
| Zn | 62.1 | 40.0 | 26.0 | 23.8 | 35.3 | 37.0 | 29.6 | - | - | - |
| Pb | 7.80 | 8.24 | 3.54 | 5.32 | 7.64 | 15.4 | 5.75 | - | - | - |
| U | 0.47 | 0.69 | 0.39 | 0.40 | 0.72 | 0.82 | 0.37 | 1.45 | 1.09 | 0.92 |
| Th | 7.26 | 5.14 | 2.81 | 2.97 | 5.52 | 7.11 | 4.11 | 3.32 | 3.37 | 3.18 |
| Nb | 8.35 | 8.21 | 4.19 | 4.86 | 6.80 | 9.50 | 6.11 | 38.0 | 36.5 | 33.6 |
| La | 26.8 | 20.3 | 13.0 | 9.82 | 19.1 | 22.5 | 17.3 | 36.9 | 34.1 | 33.7 |
| Ce | 58.3 | 44.2 | 30.2 | 22.8 | 42.0 | 46.1 | 39.0 | 77.2 | 72.9 | 74.9 |
| Pr | 7.03 | 5.35 | 3.73 | 2.77 | 5.09 | 5.51 | 4.81 | 9.37 | 9.15 | 9.28 |
| Nd | 29.3 | 22.4 | 16.2 | 11.7 | 21.3 | 22.6 | 20.7 | 37.9 | 36.6 | 40.0 |
| Sm | 6.46 | 4.95 | 3.67 | 2.65 | 4.70 | 4.96 | 4.70 | 8.06 | 8.20 | 9.11 |
| Eu | 1.33 | 1.15 | 0.91 | 0.66 | 1.06 | 1.01 | 1.12 | 1.41 | 1.85 | 2.91 |
| Gd | 6.39 | 5.03 | 4.02 | 3.03 | 4.64 | 4.93 | 5.01 | 7.69 | 7.82 | 8.87 |
| Tb | 1.00 | 0.80 | 0.67 | 0.52 | 0.72 | 0.79 | 0.82 | 1.21 | 1.22 | 1.35 |
| Dy | 5.98 | 4.98 | 4.53 | 3.71 | 4.26 | 4.84 | 5.36 | 6.57 | 7.04 | 7.04 |
| Y | 28.5 | 24.9 | 27.9 | 22.0 | 20.1 | 26.1 | 31.9 | 34.8 | 34.0 | 32.1 |
| Ho | 1.20 | 1.04 | 1.02 | 0.85 | 0.86 | 1.01 | 1.17 | 1.25 | 1.29 | 1.31 |
| Er | 3.23 | 2.94 | 3.00 | 2.59 | 2.33 | 2.82 | 3.38 | 3.11 | 3.15 | 3.20 |
| Tm | 0.45 | 0.43 | 0.46 | 0.40 | 0.34 | 0.41 | 0.50 | 0.39 | 0.40 | 0.39 |
| Yb | 2.87 | 2.93 | 3.06 | 2.76 | 2.20 | 2.69 | 3.36 | 2.28 | 2.36 | 2.28 |
| Lu | 0.43 | 0.45 | 0.49 | 0.45 | 0.33 | 0.41 | 0.53 | 0.34 | 0.32 | 0.32 |
| | 150.77 | 116.95 | 84.95 | 64.71 | 108.93 | 120.58 | 107.75 | 193.68 | 186.4 | 194.67 |
| Y/Ho | 23.75 | 23.94 | 27.35 | 25.76 | 23.29 | 25.84 | 27.26 | 27.84 | 26.36 | 24.50 |
| La/La* | 1.06 | 1.07 | 1.09 | 1.02 | 1.06 | 1.09 | 1.10 | 1.14 | 1.06 | 1.14 |
| Ce/Ce* | 0.98 | 0.98 | 0.99 | 1.00 | 0.98 | 0.95 | 0.98 | 0.98 | 0.98 | 1.01 |
| Y/Y* | 0.85 | 0.88 | 1.04 | 0.99 | 0.84 | 0.95 | 1.02 | 0.89 | 0.83 | 0.78 |
| Pr/Pr* | 1.00 | 1.00 | 0.99 | 0.99 | 1.00 | 1.00 | 0.99 | 0.97 | 0.99 | 0.95 |
| Eu/Eu* | 0.97 | 1.08 | 1.10 | 1.08 | 1.07 | 0.96 | 1.08 | 0.54 | 0.69 | 0.97 |
| $La_N/Yb_N$ | 0.69 | 0.51 | 0.31 | 0.26 | 0.64 | 0.62 | 0.38 | 10.99 | 9.82 | 10.04 |

**Supplementary Table 3 Sr-Nd isotopic data of the Baijianshan BIF**

| Sample | $^{87}Rb/^{86}Sr$ | $^{87}Sr/^{86}Sr$ | | $(^{87}Sr/^{86}Sr)_i$ | $^{147}Sm/^{144}Nd$ | $^{143}Nd/^{144}Nd$ | | $T_{DM}$(Ga) | |
|---|---|---|---|---|---|---|---|---|---|
| BJS-1 | 0.0433 | 0.717927 | 0.000004 | 0.7175 | 0.1457 | 0.512425 | 0.000006 | 1.63 | 0.65 |
| BJS-4 | 4.2608 | 0.727751 | 0.000009 | 0.6829 | 0.1308 | 0.512394 | 0.000003 | 1.39 | 1.46 |
| BJS-5 | 1.4305 | 0.728893 | 0.000008 | 0.7138 | 0.1378 | 0.512363 | 0.000003 | 1.58 | 0.19 |
| BJS-7 | 2.4192 | 0.729423 | 0.000009 | 0.7040 | 0.1473 | 0.512376 | 0.000002 | 1.78 | -0.45 |
| BJS-8 | 2.8555 | 0.718681 | 0.000003 | 0.6886 | 0.1238 | 0.512351 | 0.000004 | 1.36 | 1.27 |
| BJS-10 | 2.6390 | 0.723954 | 0.000005 | 0.6962 | 0.1344 | 0.512364 | 0.000002 | 1.51 | 0.53 |
| BJS-12 | 7.0891 | 0.740795 | 0.000007 | 0.6662 | 0.1333 | 0.512311 | 0.000003 | 1.59 | -0.40 |
| BJS-16 | 9.9936 | 0.746329 | 0.000008 | 0.6412 | 0.1334 | 0.512317 | 0.000003 | 1.58 | -0.30 |
| BJS-18 | 5.0054 | 0.731954 | 0.000008 | 0.6793 | 0.1373 | 0.51237 | 0.000004 | 1.56 | 0.38 |
| 2702H1 | 0.4737 | 0.711034 | 0.000009 | 0.7061 | 0.1286 | 0.512662 | 0.000003 | 0.88 | 6.90 |
| 2702H2 | 0.4355 | 0.711156 | 0.000009 | 0.7066 | 0.1354 | 0.512694 | 0.000006 | 0.89 | 6.88 |
| 2702H3 | 0.2322 | 0.710822 | 0.000012 | 0.7084 | 0.1377 | 0.512644 | 0.000005 | 1.02 | 5.69 |

**Supplementary Table 4 Fe isotopic data of the Baijianshan BIF**

| Sample | $^{57}Fe_{IRMM-014}$ | $^{56}Fe_{IRMM-014}$ |
|---|---|---|

| | | | | |
|---|---|---|---|---|
| BJS-2 | 2.10 | 0.09 | 1.46 | 1.46 |
| BJS-5 | 1.78 | 0.02 | 1.24 | 1.24 |
| BJS-7 | 2.76 | 0.09 | 1.89 | 1.89 |
| BJS-9 | 2.49 | 0.05 | 1.69 | 1.69 |
| BJS-12 | 3.05 | 0.04 | 2.17 | 2.17 |
| BJS-17 | 2.80 | 0.01 | 1.91 | 1.91 |

ACS